

Spin waves and transverse domain walls driven by spin waves: Role of damping

Zi-Xiang Zhao(赵梓翔), Peng-Bin He(贺鹏斌), Meng-Qiu Cai(蔡孟秋), Zai-Dong Li(李再东)

Citation: Chin. Phys. B . 2020, 29(7): 077502 . **doi:** 10.1088/1674-1056/ab90e5
Journal homepage: http://cpb.iphy.ac.cn; http://iopscience.iop.org/cpb

What follows is a list of articles you may be interested in

Nonmonotonic effects of perpendicular magnetic anisotropy on current-driven vortex wall motions in magnetic nanostripes

Su Yuan-Chang, Lei Hai-Yang, Hu Jing-Guo

Chin. Phys. B . 2015, 24(9): 097506 . **doi:** 10.1088/1674-1056/24/9/097506

Model of hybrid interfacial domain wall in ferromagnetic/antiferromagnetic bilayers

Zhang Wen, Zhai Ya, Lu Mu, You Biao, Zhai Hong-Ru, Caroline G Morgan

Chin. Phys. B . 2015, 24(4): 047502 . **doi:** 10.1088/1674-1056/24/4/047502

Angle-dependent spin waves in antidot bilayers

Hu Chun-Lian, Liao Leng, Stamps R

Chin. Phys. B . 2014, 23(12): 127501 . **doi:** 10.1088/1674-1056/23/12/127501

Effects of rotating noncircular scatterers on spin-wave band gaps of two-dimensional magnonic crystals

Yang Hui, Yun Guo-Hong, Cao Yong-Jun

Chin. Phys. B . 2014, 23(9): 097501 . **doi:** 10.1088/1674-1056/23/9/097501

Spin waves in the block checkerboard antiferromagnetic phase

Lu Feng,Dai Xi

Chin. Phys. B . 2012, 21(2): 027502 . **doi:** 10.1088/1674-1056/21/2/027502

Spin waves and transverse domain walls driven by spin waves: Role of damping*

Zi-Xiang Zhao(赵梓翔)[1], Peng-Bin He(贺鹏斌)[1,†], Meng-Qiu Cai(蔡孟秋)[1], and Zai-Dong Li(李再东)[2,3,4]

[1] School of Physics and Electronics, Hunan University, Changsha 410082, China
[2] School of Science, Tianjin University of Technology, Tianjin 300384, China
[3] State Key Laboratory of Quantum Optics and Quantum Optics Devices, Shanxi University, Taiyuan 030006, China
[4] Department of Applied Physics, Hebei University of Technology, Tianjin 300401, China

(Received 20 April 2020; revised manuscript received 20 April 2020; accepted manuscript online 7 May 2020)

Based on the uniform, helical and spiral domain-wall magnetic configurations, the excited spin waves are studied with emphasis on the role of damping. We find that the damping closes the gap of dispersion, and greatly influences the dispersion in the long-wave region for the spin waves of spiral wall and helical structure. For the uniform configuration, the Dzyaloshinskii–Moriya interaction determines the modification of dispersion by the damping. Furthermore, we investigate the interaction between spin waves and a moving spiral domain wall. In the presence of damping, the amplitude of spin wave can increase after running across the wall for small wave numbers. Driving by the spin waves, the wall propagates towards the spin-wave source with an increasing velocity. Unlike the case without damping, the relation between the wall velocity and the spin-wave frequency depends on the position of wall.

Keywords: spin waves, domain walls, helical magnetic structure, collective coordinates

PACS: 75.30.Ds, 75.60.Ch, 75.10.Hk, 75.78.–n **DOI:** 10.1088/1674-1056/ab90e5

1. Introduction

Spin waves are linear excitations on top of the stable magnetic configurations, including uniform or nonuniform ones. Magnetic domain walls are nonlinear topological excitations connecting two domains with different magnetization directions. The interplay between them has drawn much attention from the fundamental point since 1960s.[1] The research revives recent years under the background of spintronics. Roughly, the investigations have two aspects: the influences of domain walls on spin waves, and the reverse. The former includes spin-wave spectra of domain walls,[1–5] emitting of spin waves from a dynamic domain wall,[6–10] refraction and reflection of spin waves on domain walls,[11–15] phase shift of spin wave across a domain wall,[16–18] and domain-wall waveguides of spin waves,[19,20] etc. On the other hand, spin waves can drive domain walls or excite solitons by exchanging the angular momentum and linear momentum,[21–28] by the resonance between spin waves and internal modes of walls,[29–32] and by the interference of spin waves.[33]

To understand the dynamics of domain walls driven by spin waves, the collective-coordinate method is a good choice, which can get the key physical features with qualitative clarity. There exist transfers of momentum and angular momentum between the magnon currents and the domain walls. Similar to the spin-transfer effects generated the spin-polarized current, the spin-wave-related driven terms can be introduced into the dynamic equations of collective coordinates.[23,34] Furthermore, the spin-wave excitations can also be involved into the Landau–Lifshitz–Gilbert (LLG) equation as driving terms. The dynamic equations about the collective coordinates of domain walls can be derived directly through perturbative expansion about the amplitude of spin waves.[6,35]

In previous studies, the influences of damping, on both the spin waves and the domain walls driven by spin waves, are often neglected or not fully considered, especially in the analytic calculations. For example, in Refs. [23,34], only the influence of damping on the moving domain wall is considered, whereas the effect on the spin waves is ignored. In Ref. [35], the damped spin waves are included, while the influence of the spin-wave attenuation on the domain-wall velocity is neglected.

In this paper, considering a ferromagnetic film with a bulk Dzyaloshinskii–Moriya interaction (DMI) and an in-plane uniaxial magnetic anisotropy, we investigate the dispersion and attenuation of spin waves on top of the uniform, spiral domain-wall, and helical magnetic configurations. Then, the dynamics of a transverse domain wall driven by spin waves is studied by the collective coordinates method. During the analysis, the role of damping is emphasized.

*Project supported by the National Natural Science Foundation of China (Grant Nos. 61774001 and 51972103), the Natural Science Foundation of Hebei Province of China (Grant No. F2019202141), and the Fund of the State Key Laboratory of Quantum Optics and Quantum Optics Devices, Shanxi University, China (Grant No. KF201906).

†Corresponding author. E-mail: hepengbin@hnu.edu.cn

© 2020 Chinese Physical Society and IOP Publishing Ltd

2. Model and static magnetic configurations

Assuming uniform magnetization within the cross section of a magnetic nanowire, a one-dimensional model is employed along the z-axis, as shown in Fig. 1. Including the exchange energy, bulk DMI, energy of in-plane uniaxial magnetic anisotropy, and demagnetization energy, the total magnetic energy per unit area (in the xy plane) reads

$$E = \int \left[\left(\frac{\partial \boldsymbol{m}}{\partial z} \right)^2 - \kappa m_z^2 + 2d\boldsymbol{m} \cdot \left(\boldsymbol{e}_z \times \frac{\partial \boldsymbol{m}}{\partial z} \right) + \mathcal{E}_\mathrm{d} \right] \mathrm{d}z, \quad (1)$$

where $\boldsymbol{m}$ is the normalized magnetization vector, and $\mathcal{E}_\mathrm{d} = \frac{1}{2}(N_x m_x^2 + N_y m_y^2)$ is the density of demagnetization energy. The dimensionless parameters $d = D/(2\sqrt{A\mu_0 M_\mathrm{s}^2})$ and $\kappa = K/(\mu_0 M_\mathrm{s}^2)$ with D being the DMI constant, K the anisotropy constant, μ_0 the vacuum permeability, M_s the saturation magnetization, and A the exchange constant. N_x and N_y are the demagnetization factors. Additionally, the magnetization dynamics is governed by the LLG equation

$$\frac{\partial \boldsymbol{m}}{\partial t} = \boldsymbol{m} \times \frac{\delta E}{\delta \boldsymbol{m}} + \alpha \boldsymbol{m} \times \frac{\partial \boldsymbol{m}}{\partial t}, \quad (2)$$

where α is the Gilbert damping constant. In the above equations, the time and length have been nondimensionalized, in which natural units are taken as $t_0 = 1/(\gamma_0 M_\mathrm{s})$ and $l_0 = \sqrt{A/(\mu_0 M_\mathrm{s}^2)}$ with $\gamma_0 = \mu_0 |e|/m_e$ being the gyromagnetic ratio.

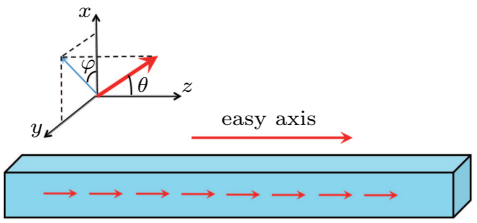


Fig. 1. Model and coordinates system.

In order to solving the static equation $\boldsymbol{m} \times \frac{\delta E}{\delta \boldsymbol{m}} = 0$, it is convenient to take the spherical coordinates defined by $\boldsymbol{e}_r = \boldsymbol{m}$, $\boldsymbol{e}_\theta = \cos\theta\cos\varphi \boldsymbol{e}_x + \cos\theta\sin\varphi \boldsymbol{e}_y - \sin\theta \boldsymbol{e}_z$, and $\boldsymbol{e}_\varphi = -\sin\varphi \boldsymbol{e}_x + \cos\varphi \boldsymbol{e}_y$, with θ and φ being the polar and azimuthal angles, respectively. Then, after obtaining the static solutions, we compare their energies and acquire three kinds of stable magnetic configurations. One is the uniform solution $\theta = 0$ or π under $d^2 < \kappa$, which is just the ferromagnetic ground state. The other is a spiral domain wall for $d^2 < \kappa$,[36,37]

$$\theta = 2\arctan\exp\left(\lambda \frac{z}{\Delta}\right), \quad (3)$$

$$\varphi = \Gamma z + \phi, \quad (4)$$

where the wall width parameter $\Delta = 1/\sqrt{\kappa - d^2}$, $\Gamma = d$ and $2\pi/\Gamma$ is the pitch of spiral; $\lambda = \pm 1$ correspond to the boundary conditions that $\theta = 0, \pi$ for $z \to \mp\infty$ and $\theta = \pi, 0$ for $z \to \mp\infty$, respectively. For $d^2 > \kappa$, a helical structure emerges, $\theta = \pm\pi/2$, $\varphi = \mathrm{d}z + \phi$.[36,38] Here, we assume a square cross section, namely, the aspect ratio is about one. Thus, $N_x \approx N_y$.[39] Under this approximation, ϕ is undetermined. The demagnetization energy comes in only through replacing κ by $\kappa_\mathrm{eff} = \kappa + N_x$. For wall solution, the demagnetization only affects the wall width. For brevity, we still take κ denoting the effect anisotropy in the following sections.

3. Spin waves excited on static configurations

3.1. Spin waves of uniform configuration

For the uniform configuration, $\theta_0 = 0$ or π. In the linear regime, the spin wave is described by a small fluctuation that leads to $\boldsymbol{m} = \lambda \boldsymbol{e}_z + u(z,t)\boldsymbol{e}_x + v(z,t)\boldsymbol{e}_y$, with $\lambda = \pm 1$. Inserting this ansatz into Eq. (2) and keeping the leading-order terms, the spin wave solution can be obtained,

$$u = \rho\, \mathrm{e}^{-\mathrm{sgn}(v_\mathrm{g})\frac{z}{\Lambda}}\, \mathrm{e}^{\mathrm{i}(-\omega t + kz + \zeta)}, \quad (5)$$

$$v = \rho\, \mathrm{e}^{-\mathrm{sgn}(v_\mathrm{g})\frac{z}{\Lambda}}\, \mathrm{e}^{\mathrm{i}\left(-\omega t + kz + \zeta + \lambda\frac{\pi}{2}\right)}, \quad (6)$$

where ρ is the amplitude, Λ is the attenuation length, ω is the frequency, k is the wave number, ζ is the initial phase, sgn denotes sign function, and $v_\mathrm{g} = \partial\omega/\partial k$ is the group velocity of spin wave. Here the attenuation due to damping is taken into account. Obviously, the spin waves are circular polarized and right-rotated.

In general, the attenuation length must be positive and decrease with the damping increasing. Namely, $\Lambda > 0$ and $\partial\Lambda/\partial\alpha < 0$. Under these conditions, the dispersion relation can be obtained as follows:

$$\omega = \frac{4}{\alpha^2}\left[\sqrt{k'^4 + \alpha^2 k'^2\left(k'^2 + \kappa - d^2\right)} - k'^2\right], \quad (7)$$

where $k' = k + \lambda d$. The corresponding attenuation length is $\Lambda = 4|k'|/(\alpha\omega)$. In Fig. 2, the frequency, attenuation length, and group velocity versus the wave number k are illustrated for $\lambda = 1$. It can be found that the damping greatly changes the dispersion relation around $k = -\lambda d$, as shown in Fig. 2(a). In the absence of damping, the dispersion relation is parabolic, $\omega = 2[(k + \lambda d)^2 + \kappa - d^2]$, which can be obtained by taking $\alpha \to 0$ in Eq. (7). Meanwhile, a gap exists at $k = -\lambda d$ without the damping. In addition, in this region, the group velocity is sharply increased in the presence of damping, as shown in Fig. 2(b). When k approaches $-\lambda d$ from the right (left) along the axis, the group velocity reaches $v_\mathrm{max}(-v_\mathrm{max})$ with $v_\mathrm{max} = 4\sqrt{\kappa - d^2}/\alpha$. At $k = -\lambda d$, the group velocity is zero. The corresponding attenuation length is $\sqrt{1/(\kappa - d^2)}$. Without damping, the group velocity depends on k linearly, $v_\mathrm{g} = 4(k + \lambda d)$. In the presence of DMI, the dispersion curve is moved along the k axis. This point can be used to determine the strength of DMI and provide a nonreciprocal spin-wave channel experimentally.[40–43]

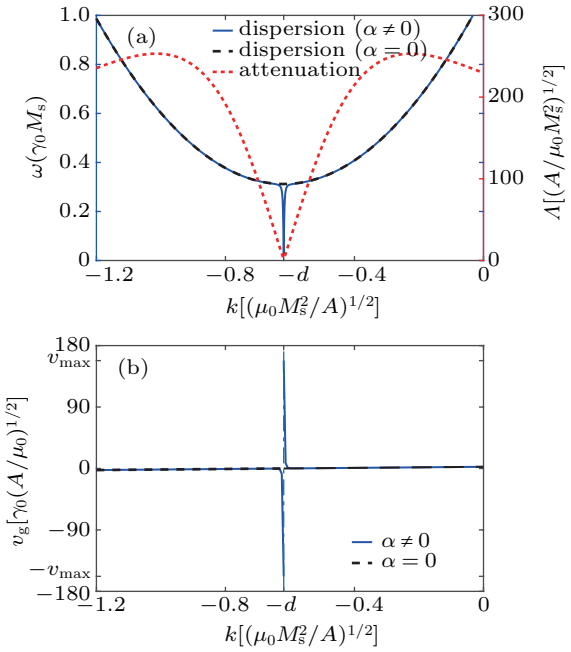


Fig. 2. (a) Dispersion and attenuation of the spin wave excited on top of uniform configuration ($\theta_0 = 0$). The solid curve represents the dispersion relation with damping, while the dashed curve without damping. The dotted curve denotes the attenuation length as a function of wave number. (b) Group velocity. The solid and dashed curves correspond to the cases with and without damping, respectively. Here we take typical magnetic parameters: the Gilbert damping $\alpha = 0.01$, the exchange constant $A = 8.78 \times 10^{-12}$ J/m, the saturation magnetization $M_s = 3.84 \times 10^5$ A/m, the anisotropy constant $K = 10^5$ J/m^3, the DMI constant $D = 1.58 \times 10^{-3}$ J/m^2. From these parameters, the dimensionless anisotropy and DMI constants are $\kappa = K/(\mu_0 M_s^2) = 0.54$ and $d = D/(2\sqrt{A\mu_0 M_s^2}) = 0.62$. The natural units of frequency, velocity and wave number are $\gamma_0 M_s = 8.49 \times 10^{10}$ Hz, $\gamma_0\sqrt{A/\mu_0} = 584$ m/s and $\sqrt{\mu_0 M_s^2/A} = 1.45 \times 10^8$ m^{-1}.

There is an intuitive physical picture which can explain the gapped spectrum for $\alpha = 0$ and gapless one for $\alpha \neq 0$. For ease of interpretation, we neglect the DMI firstly and the bottom of spectrum is at $k = 0$. Without damping, if there is no anisotropy, the system is rotational symmetric. According to the Nambu–Goldstone theorem, the spin wave is gapless and a massless mode exists. Here $k = 0$ means that all spins are uniformly twisted. If rotating all spin uniformly, the total exchange energy is unchanged. Thus, no energy is costed when exciting this Goldstone mode. Including the magnetic anisotropy, to rotate every spin uniformly, there exists an energy cost to overcome the anisotropy. Therefore, a gap opens and is measured by the anisotropy parameter 2κ. Restoring the dimension, the gap is $\mu_0 H_K M_s$ with $H_K = 2K/M_s$ being the anisotropy field. This is just the work done by the anisotropy field.

In the presence of damping, there exists a massless mode (zero mode) expressed as

$$\boldsymbol{m} = \boldsymbol{e}_z + \rho\, \mathrm{e}^{-\mathrm{sgn}(v_g)\frac{z}{\Lambda}} \left[\cos(\mathrm{d}z + \zeta)\boldsymbol{e}_x + \sin(\mathrm{d}z + \zeta)\boldsymbol{e}_y\right]. \quad (8)$$

As discussed above, if rotating all spins uniformly, there is no energy cost, namely, the total energy is unchanged. Because the angles between adjacent spins are unchanged, the exchange energy is unchanged when exciting this mode. In general, the Gilbert damping in magnet results from the coupling between spins and lattice. The damping torque $\alpha \boldsymbol{m} \times \partial \boldsymbol{m}/\partial t$ points toward the easy axis ($\boldsymbol{e}_z$). If a spin rotates around the easy axis with a constant precession angle, the anisotropy energy will not change and the damping will not work. Thus, there is no energy cost. If the precession angle is increased, the anisotropy energy increases. However, because the damping torque does negative work, the incremental anisotropy energy can be provided by the lattice. There is also no energy cost. Similarly, when decreasing the precession angle, the damping torque does positive work, and the reduction of anisotropy energy is transferred to the lattice. Anyway, a uniform twist of all spins cannot cost energy. This leads to a massless mode in a magnetic system with the exchange coupling, the magnetic anisotropy and the Gilbert damping.

Now, let us analyze the role of DMI which has two features: exchange and anisotropy. This can be observed by rewrite the energy density Eq. (1) in the form: $\mathcal{E} = [\frac{\partial \boldsymbol{m}}{\partial z} + d(\boldsymbol{m} \times \boldsymbol{e}_z)]^2 - (\kappa - d^2)m_z^2 - d^2$. The second term indicates that DMI changes the anisotropy effectively. This leads to the change of gap from 2κ to $2(\kappa - d^2)$. For spin wave based on the uniform ground state, the bottom of spectrum corresponds to the minimum of the term $[\frac{\partial \boldsymbol{m}}{\partial z} + d(\boldsymbol{m} \times \boldsymbol{e}_z)]^2$. Therefore, one has an equation $\frac{\partial \boldsymbol{m}}{\partial z} = -d(\boldsymbol{m} \times \boldsymbol{e}_z)$. Inserting the spin wave ansatz into this equation, one has $k = -d$. Without DMI, the bottom of spectrum is at $k = 0$. With DMI, the exchange coupling is altered and the bottom moves to $k = -d$.

Finally, when the Gilbert parameter α increases, the width of the peak in Fig. 2(a) increases. For small k, the exchange energy is low. Thus, the influence of damping is great. With k increasing, the exchange energy increases. Correspondingly, the influence of damping becomes increasingly weaker. The damping influences the spectrum obviously in the long-wave region.

3.2. Spin waves of spiral domain wall

In the domain-wall region, the magnetization is nonuniform. It is convenient to take a rotating reference frame attached on the magnetization of domain wall with the unit vectors $\boldsymbol{e}_r = \boldsymbol{m}_0 = \sin\theta_0 \cos\varphi_0 \boldsymbol{e}_x + \sin\theta_0 \sin\varphi_0 \boldsymbol{e}_y + \cos\theta_0 \boldsymbol{e}_z$. Here θ_0 and φ_0 take the Walker profile expressed by Eqs. (3) and (4), respectively. The spin wave is assumed as $\boldsymbol{m} = \boldsymbol{m}_0 + u\boldsymbol{e}_\theta + v\boldsymbol{e}_\varphi$ under the linear approximation. Inserting this ansatz into the LLG equation (Eq. (2)) and keeping only the linear terms, the spin waves obey

$$\frac{\partial u}{\partial t} + \alpha\frac{\partial v}{\partial t} = -2\left[\hat{H} + \Delta^{-2}\right]v, \quad (9)$$

$$-\frac{\partial v}{\partial t} + \alpha\frac{\partial u}{\partial t} = -2\left[\hat{H} + \Delta^{-2}\right]u, \quad (10)$$

where $\hat{H} = -\partial^2/\partial z^2 - (2/\Delta^2)\mathrm{sech}^2(z/\Delta)$, with the second term being the Pöschl–Teller potential. Using the eigenfunction of the Pöschl–Teller potential,[44] the spin wave solutions are calculated,

$$u = A\,\mathrm{e}^{-\mathrm{sgn}(v_g)\frac{z}{\Lambda}}\,\mathrm{e}^{\mathrm{i}(-\omega t+kz+\zeta)}, \tag{11}$$

$$v = A\,\mathrm{e}^{-\mathrm{sgn}(v_g)\frac{z}{\Lambda}}\,\mathrm{e}^{\mathrm{i}\left(-\omega t+kz+\zeta+\frac{\pi}{2}\right)}, \tag{12}$$

where the amplitude is dependent on the wave vector and space coordinate,

$$A(k,z) = \rho\sqrt{\frac{[\tanh(\frac{z}{\Delta})+\frac{\Delta}{\Lambda}]^2+\Delta^2k^2}{(1-\frac{\Delta}{\Lambda})^2+\Delta^2k^2}}, \tag{13}$$

with ρ being an arbitrary parameter determined by the perturbation. And so is the phase shift,

$$\zeta(k,z) = \arctan\left\{\frac{\Delta k[\tanh(\frac{z}{\Delta})+1]}{\Delta^2k^2+(\frac{\Delta}{\Lambda}-1)[\frac{\Delta}{\Lambda}+\tanh(\frac{z}{\Delta})]}\right\}. \tag{14}$$

The dispersion and attenuation are

$$\omega = \frac{4[\sqrt{k^4+\alpha^2k^2(k^2+\Delta^{-2})}-k^2]}{\alpha^2}, \tag{15}$$

and $\Lambda = 4|k|/(\alpha\omega)$. It is worth noting that the dispersion is similar to that of uniform configuration (Eq. (7)) apart from a translation of λd along the k axis. In the long-wave limit ($k \to 0$), the dispersion is greatly reshaped by the damping and the gap is closed. Meanwhile, the attenuation length approaches the wall width parameter Δ.

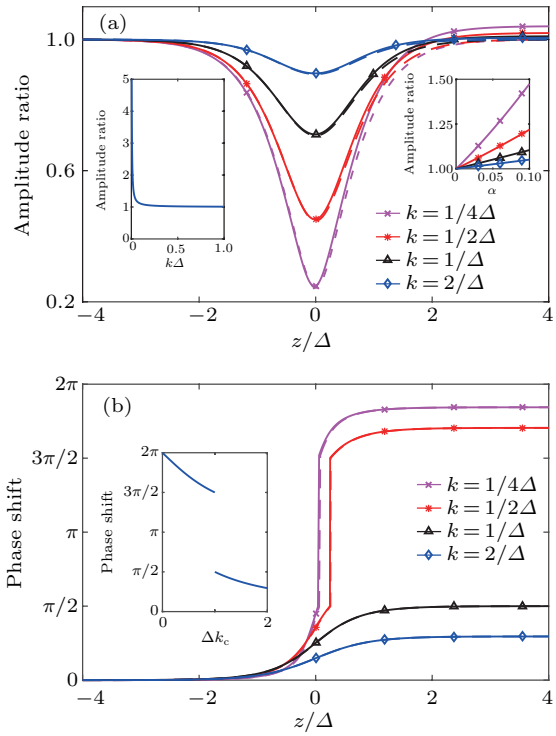


Fig. 3. The amplitude ratio (a) and phase shift (b) of spin wave along the domain wall for different wave numbers. The solid lines correspond to the case of $\alpha = 0.01$, and the dashed lines to $\alpha = 0$. The insets show the total amplitude ratio and phase shift across the domain wall. The rest parameters are the same as those in Fig. 2. Thus, the domain width $\Delta = 1/\sqrt{\kappa - d^2} = 2.53$ in dimensionless form or 1.74×10^{-8} m after restoring the dimension.

Going through the domain wall, the amplitude of spin wave changes, which is attributed to the Pöschl–Teller potential and the attenuation. Figure 3(a) shows the amplitude ratio due to the Pöschl–Teller potential. Across the domain wall, the amplitude increases with a factor $\sqrt{[(1+\Delta/\Lambda)^2+\Delta^2k^2]/[(1-\Delta/\Lambda)^2+\Delta^2k^2]}$. In the absence of damping, $\Lambda \to \infty$, this factor is 1. The amplitude is unchanged, as manifested by the dashed lines in Fig. 3(a). In the presence of damping, this factor is greater than 1 and increases with the damping, as indicated in the right inset of Fig. 3(a). With k decreasing, this factor increases. As shown in the left inset of Fig. 3(a), for small k, this factor becomes very large because $\Lambda \to \Delta$ under $k \to 0$. For large k, this factor approaches 1.

Taking the domain-wall width as $\pi\Delta$,[45] the attenuation contributes a factor $\exp(-\pi\Delta/\Lambda)$ to the amplitude ratio. Hence, the amplitude changes approximately by a factor of $\sqrt{[(1+\Delta/\Lambda)^2+\Delta^2k^2]/[(1-\Delta/\Lambda)^2+\Delta^2k^2]}\exp(-\pi\Delta/\Lambda)$ when the spin wave goes across the domain wall. In the long-wave limit, this amplitude ratio is about $2\mathrm{e}^{-\pi}\alpha/(\Delta k)$ by keeping the leading term of k. Here, the amplitude possibly increases after across the domain wall in the presence of damping. For large k, the amplitude ratio due to the Pöschl–Teller potential approaches to 1, and the attenuation determines the change of amplitude. Across the wall, the spin-wave amplitude decreases with a factor $\exp[-\pi\Delta k(\sqrt{1+\alpha^2}-1)/\alpha]$ approximately.

Additionally, the phase also changes with the spin wave passing across the domain wall, as shown in Fig. 3(b). There exists a critical wave number $k_c = 1/(\sqrt{1+\alpha^2}\Delta)$, for which the corresponding wave length is about Δ. Above k_c, the phase continuously varies in the domain wall. Below k_c, the phase is reversed across the center of domain wall. The dependence of total phase shift on the wave number k is shown in the inset of Fig. 3(b). The total phase shift is $\arctan[2k\Delta/(-1+k^2\Delta^2+\Delta^2/\Lambda^2)]$. Here k_c can be obtained by solving $-1+k^2\Delta^2+\Delta^2/\Lambda^2 = 0$. At k_c, the total phase shift jumps from $3\pi/2$ to $\pi/2$. With k increasing, the total phase shift decreases and approaches 0 when $k \to \infty$. Without damping, $\alpha = 0$ and $\Lambda = \infty$, $k_c = 1/\Delta$. Comparing the dashed and solid curves in Fig. 3(b), one can find that damping has weak effect on the phase shift.

3.3. Spin waves of helical structure

For strong DMI, $d^2 > \kappa$, there exists a static helical structure, which is described by $\theta_0 = \pm\pi/2$, and $\varphi_0 = \mathrm{d}z + \phi$. Adopting the rotating reference frame attached on the helical magnetization with $\boldsymbol{e}_r = \boldsymbol{m}_0$, the linear spin wave is expressed as $\boldsymbol{m} = \boldsymbol{m}_0 + u\boldsymbol{e}_\theta + v\boldsymbol{e}_\varphi$. Inserting this ansatz into Eq. (2) and keeping only the linear terms, the spin wave solutions can be

written as

$$u = \rho_u \mathrm{e}^{-\mathrm{sgn}(v_g)\frac{z}{\Lambda}} \mathrm{e}^{\mathrm{i}(-\omega t+kz+\zeta)}, \quad (16)$$

$$v = \rho_v \mathrm{e}^{-\mathrm{sgn}(v_g)\frac{z}{\Lambda}} \mathrm{e}^{\mathrm{i}\left(-\omega t+kz+\zeta+\frac{\pi}{2}\right)}. \quad (17)$$

The dispersion relation is

$$\omega = \frac{2\sqrt{2}|k|}{\alpha^2}\sqrt{f-\sqrt{f^2-4\alpha^4k^2\left[k^2+(d^2-\kappa)\right]}}, \quad (18)$$

with $f = 4k^2+2\alpha^2k^2+\alpha^2\left(d^2-\kappa\right)$, and the corresponding attenuation length is $\Lambda = 4|k|/(\alpha\omega)$. The damping affects the dispersion relation and group velocity greatly in the long-wave region. As shown in Fig. 4(a), there is no gap for the dispersion with and without damping. This can be understood by the Nambu–Goldstone theorem. For strong DMI, there exists a breaking of axis symmetry and the ground state is one of the degenerate ones, $\varphi_0 = \mathrm{d}z+\varphi$, where φ could be arbitrary. When one of the degenerate ground state is chosen, there should be a corresponding Goldstone mode.

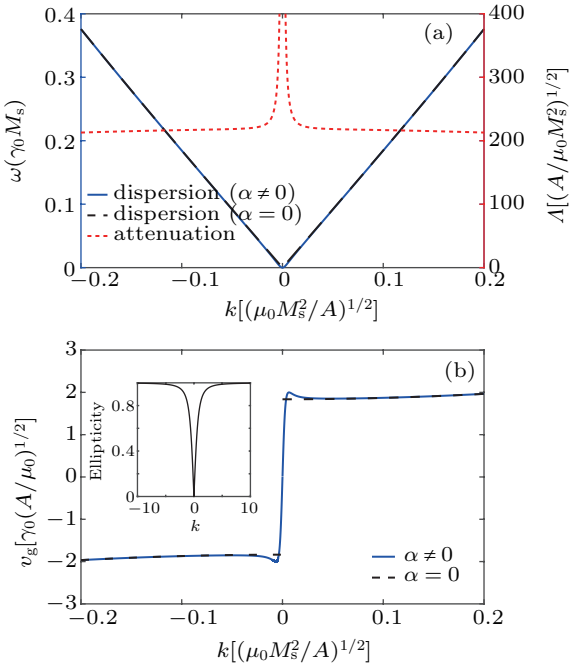


Fig. 4. (a) Dispersion and attenuation of spin wave excited on top of helical configuration. The solid curve represents the dispersion relation with damping, while the dashed curve without damping. The dotted curve denotes the attenuation length as a function of wave number. (b) Group velocity. The solid and dashed curves correspond to the cases with and without damping, respectively. The inset in (b) shows the dependence of ρ_u/ρ_v on k. Here the same parameters are used as those in Fig. 2 except the DMI parameter $D = 3\times10^{-3}$ J/m^2 which ensures $d^2 > \kappa$.

Unlike the spin wave excited on top of uniform configuration, the attenuation length is very large in the long-wave region. Without damping, the dispersion relation is $\omega = 2|k|\sqrt{k^2+(d^2-\kappa)}$. In the presence of damping, as shown in Fig. 4(b), the group velocity varies continuously with k and approaches zero when $k\to0$. In the absence of damping, the group velocity changes sign with k across zero and approaches $\pm2\sqrt{d^2-\kappa}$ when $k\to0^{\pm}$.

In contrast with the spin waves excited on top of the uniform and domain-wall configurations, an elliptic spin wave is excited on the helical configuration. The ellipticity (defined as ρ_u/ρ_v) varies with the wave number,

$$\frac{\rho_u}{\rho_v} = \frac{2\sqrt{2}k^2}{\sqrt{8k^4+\left(g+\sqrt{g^2+16\alpha^2k^4}\right)\left(d^2-\kappa\right)}}, \quad (19)$$

with $g = 4k^2+\alpha^2(d^2-\kappa)$. Apart from the long-wave region ($k\to0$), the damping hardly influences the polarization of spin wave. As shown in the inset of Fig. 4(b), in the long-wave limit ($k\to0$), $\rho_u/\rho_v\to0$, the spin wave is linear polarized. In the short-wave region, $\rho_u/\rho_v\to1$, the spin wave is circular polarized.

4. Dynamic domain wall driven by spin waves

Based on the static spiral profile (Eqs. (3) and (4)) and taking the center position q and magnetization angle ϕ of domain wall as dynamic variables, we have

$$\theta_0(z,t) = 2\arctan\exp\left[\lambda\frac{z-q(t)}{\Delta}\right], \quad (20)$$

$$\varphi_0(z,t) = \Gamma\left[z-q(t)\right]+\phi(t). \quad (21)$$

Excited on this dynamic domain wall, the spin wave reads $\boldsymbol{m} = \boldsymbol{m}_0+\boldsymbol{m}'$, with $\boldsymbol{m}' \approx -1/2\left[u^2(z,t)+v^2(z,t)\right]\boldsymbol{e}_r + u(z,t)\boldsymbol{e}_\theta+v(z,t)\boldsymbol{e}_\varphi$ up to to the second order of u and v. Here a moving coordinate system is taken with $\boldsymbol{e}_r = \boldsymbol{m}_0$. Inserting this ansatz and the spin wave solutions (11) and (12) into the LLG equation (2) and keeping the terms up to the second order of the amplitude ρ, we get the dynamic equations about q and ϕ as follows:

$$\begin{pmatrix} a_{11} & a_{12} \\ a_{21} & a_{22} \end{pmatrix}\begin{pmatrix} \frac{\lambda}{\Delta}\frac{\mathrm{d}q}{\mathrm{d}t} \\ \Gamma\frac{\mathrm{d}q}{\mathrm{d}t}-\frac{\mathrm{d}\phi}{\mathrm{d}t} \end{pmatrix} = \begin{pmatrix} b_1 \\ b_2 \end{pmatrix}, \quad (22)$$

where

$$\begin{aligned} a_{11} =& -2-\lambda(I_1+\alpha I_2)\rho\exp[-(q-q_s)/\Lambda] \\ & -(\alpha I_3-I_4)\rho^2\exp[-2(q-q_s)/\Lambda], \\ a_{12} =& -2\alpha+\lambda(\alpha I_1-I_2)\rho\exp[-(q-q_s)/\Lambda] \\ & +\alpha I_5\rho^2\exp[-2(q-q_s)/\Lambda], \\ a_{21} =& -2\alpha-\lambda(\alpha I_1-I_2)\rho\exp[-(q-q_s)/\Lambda] \\ & +\alpha I_6\rho^2\exp[-2(q-q_s)/\Lambda], \\ a_{22} =& 2-\lambda(I_1+\alpha I_2)\rho\exp[-(q-q_s)/\Lambda] \\ & -(\alpha I_3+I_4)\rho^2\exp[-2(q-q_s)/\Lambda], \\ b_1 =& \frac{4\lambda}{\Delta^2}\rho^2\exp[-2(q-q_s)/\Lambda]I_7, \\ b_2 =& \frac{8\lambda}{\Delta^2}\rho^2\exp[-2(q-q_s)/\Lambda]I_8. \end{aligned}$$

Here q_s is the position of the spin-wave source, and ρ is an amplitude parameter determined by the wave source. The detailed derivations and the parameters I_{1-8} are listed in Appendix A.

Up to the order of ρ^2, the dynamic equations of q and ϕ can be simplified to

$$\frac{\mathrm{d}q}{\mathrm{d}t} = -\mathcal{V}(k)\rho^2 \mathrm{e}^{-2\frac{q-q_s}{\Lambda}}, \tag{23}$$

$$\frac{\mathrm{d}\phi}{\mathrm{d}t} = -\mathcal{W}(k)\rho^2 \mathrm{e}^{-2\frac{q-q_s}{\Lambda}}, \tag{24}$$

where $\mathcal{V}(k) = [(2k)/(1+\alpha^2)][1-\Delta^2/\Lambda^2+\Delta^2k^2+2\alpha\Delta^2k/\Lambda]/[(1-\Delta/\Lambda)^2+\Delta^2k^2)][(\pi\Delta/\Lambda)\csc(\pi\Delta/\Lambda)]$, and $\mathcal{W}(k) = (\Gamma-\lambda\alpha/\Delta)\mathcal{V}(k)$. Then, the position and velocity of domain wall can be obtained as follows:

$$q = q_0 + \frac{\Lambda}{2}\ln\left(1+\frac{2v_0t}{\Lambda}\right), \tag{25}$$

$$v_w = \frac{v_0}{1+\frac{2v_0t}{\Lambda}}, \tag{26}$$

where q_0 is the initial position, and $v_0 = -\mathcal{V}(k)\rho^2\exp[-2(q_0-q_s)/\Lambda]$ is the initial velocity. Without damping, the velocity is independent of the position of domain wall. Taking $\alpha = 0$ and $\Lambda \to \infty$, the velocity becomes $-2k\rho^2$, and the angular velocity $d\phi/dt = -2k\Gamma\rho^2$.

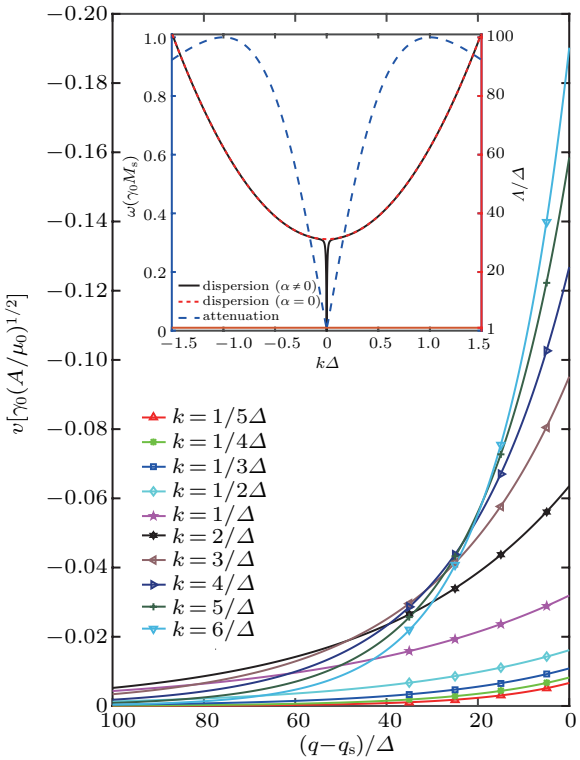


Fig. 5. Dependence of velocity of domain wall on its distance from the source of spin wave for different wave numbers. The inset shows the dispersion relations with and without damping, as well as the dependence of attenuation length on the wave number. Here the Gilbert damping constant $\alpha = 0.01$. The amplitude parameter $\rho = 0.2$. The rest parameters are the same as those in Fig. 3. Thus, the domain width Δ is 1.74×10^{-8} m after restoring the dimension and the natural unit of velocity is $\gamma_0\sqrt{A/\mu_0} = 584$ m/s.

Taking the initial position $q_0 = q_s + 100\Delta$, we plot the variation of domain-wall velocity with its position for different wave numbers in Fig. 5. Obviously, the domain wall runs opposite to the spin wave. In our model, there is no reflection of spin wave across the domain wall, as shown in Fig. 3. Therefore, the transfer of angular momentum leads to the opposite motion directions of domain wall and spin wave.[21] In addition, the velocity increases with time. This point is easy to be understood. When the domain wall approaches the source of spin wave, the attenuation of spin wave becomes smaller. Thus, the velocity becomes larger.

Up to the order of ρ^4, there is no simple analytic expression for velocity. The dynamic equation of q and its numeric solution are placed in Appendix B. The result is shown in Fig. B1 in Appendix B. Comparing Fig. 5 and Fig. B1, it can be found that they are similar on the evolution of velocity, except that there appears to be some small oscillations when the equation is accurate to ρ^4.

There are two aspects of the influences of damping on the spin wave. Firstly, the dispersion is greatly moderated in the long-wave region ($k \to 0$), as shown in the inset of Fig. 5. Secondly, the damping results in the attenuation of spin wave. The attenuation length is close to Δ as $k \to 0$, and reaches the maximum $\sqrt{1+\alpha^2}\Delta/\alpha$ at $k = 1/(\sqrt{1+\alpha^2}\Delta)$. Above this maximum, the attenuation length decreases with k increased and approaches 0 for $k \to \infty$. In Ref. [35], the calculation is carried out under the condition $\Lambda \gg \Delta$ and by keeping the lowest non-vanishing order in α. This case corresponds to the region that k is around $1/\Delta$. In this region, the dispersion is scarcely influenced by the damping. In the long-wave region, it is unsuitable to omit the higher order of α.

In the presence of damping, the velocity of domain wall depends on the wave number (frequency) of spin wave more complexly. Due to the attenuation of spin wave, apart from the function $\mathcal{V}(k)$ in Eq. (23), the velocity relies on k through the factor $\exp[-2(q-q_s)/\Lambda]$, where the attenuation length Λ is a function of k. For different positions of domain wall, the relations between the velocity and the wave number are different. As shown in Fig. 5, near the source of spin wave, the velocity of domain wall increases with wave number (frequency). Far from the source, there is no simple relation. In the absence of damping, the velocity is proportional to the wave number.

5. Conclusions

We have investigated the spin waves excited on top of uniform, spiral domain-wall and helical magnetic configurations in the film with an in-plane magnetic anisotropy and a bulk DMI. We put emphasis on the role of damping. For the spin wave of uniform configuration, the dispersion is greatly modified by the damping around $k = -\lambda D/(2A)$ and the gap is closed. The group velocity becomes very large with a maximum $\gamma_0/(\mu_0 M_s)\sqrt{4KA-D^2}/(4\alpha)$ (about several km/s). For the spin wave of domain wall, the gap of dispersion is closed at

the long-wave limit. The attenuation length can reach a maximum Δ/α when the wave length amounts to the width of wall roughly. Especially, the amplitude of spin wave can increase after running across the wall in the presence of damping for small wave number. For the spin wave of helical structure, the damping also modifies the dispersion greatly in the long-wave region, and the attenuation length becomes very large here. Unlike the spin waves of uniform and wall configurations, the spin wave of helical structure is elliptically polarized. In the presence of damping, there exist gapless modes for the three kinds of spin waves. Qualitatively, combined with symmetry analysis, this phenomenon is interpreted by the variation of energy when exciting the modes.

The effect of spin waves on the moving spiral domain wall is also studied by the collective-coordinate method. We find that driven by a spin wave the velocity of domain wall is not a constant in the presence of damping. The domain wall moves towards the source of spin wave and the velocity increases. Considering the attenuation of spin wave, the relation between the wall velocity and the wave number of spin wave depends on the position of wall.

Appendix A: Derivation of the q–ϕ model

Here q–ϕ equations of domain wall with spin waves are derived from the LLG equation,

$$\begin{aligned}&\frac{\partial \boldsymbol{m}}{\partial t}-\alpha \boldsymbol{m}\times\frac{\partial \boldsymbol{m}}{\partial t}\\&=-2\boldsymbol{m}\times\frac{\partial^2 \boldsymbol{m}}{\partial z^2}-2\kappa(\boldsymbol{m}\cdot\boldsymbol{e}_z)(\boldsymbol{m}\times\boldsymbol{e}_z)\\&\quad+4d\boldsymbol{m}\times\left(\boldsymbol{e}_z\times\frac{\partial \boldsymbol{m}}{\partial z}\right).\end{aligned}\tag{A1}$$

It is assumed that the head-to-head (or tail-to-tail) domain wall remains the Walker profile, $\boldsymbol{m}_0=\sin\theta_0\cos\varphi_0\boldsymbol{e}_x+\sin\theta_0\sin\varphi_0\boldsymbol{e}_y+\cos\theta_0\boldsymbol{e}_z$, with θ_0 and φ_0 being $\theta_0(z,t)=2\arctan\exp[\lambda(z-q(t))/\Delta]$, $\varphi_0(z,t)=\Gamma[z-q(t)]+\phi(t)$. Considering the linear spin wave excited on the dynamic domain wall, $\boldsymbol{m}=\boldsymbol{m}_0+\boldsymbol{m}'$. By taking the moving coordinate system attached on the magnetization of domain wall with $\boldsymbol{e}_r=\boldsymbol{m}_0$, $\boldsymbol{e}_\theta=-\sin\theta_0\boldsymbol{e}_x+\cos\theta_0\cos\varphi_0\boldsymbol{e}_y+\cos\theta_0\sin\varphi_0\boldsymbol{e}_z$, and $\boldsymbol{e}_\varphi=-\sin\varphi_0\boldsymbol{e}_y+\cos\varphi_0\boldsymbol{e}_z$, the spin wave is expressed as $\boldsymbol{m}'\approx-1/2\left[u^2(z,t)+v^2(z,t)\right]\boldsymbol{e}_r+u(z,t)\boldsymbol{e}_\theta+v(z,t)\boldsymbol{e}_\varphi$. Inserting this spin wave ansatz into the LLG equation (A1) and integrating over z, we can reach the dynamic equations of q and ϕ. Firstly, For the Walker ansatz, we have $\theta_{0t}=-\lambda\sin\theta_0\frac{q_t}{\Delta}$, $\varphi_{0t}=-\Gamma q_t+\phi_t$, $\theta_{0z}=\frac{\lambda}{\Delta}\sin\theta_0$, $\theta_{0zz}=\frac{1}{\Delta^2}\sin\theta_0\cos\theta_0$, and $\varphi_{0z}=\Gamma$. The subscript in f_t (f_z) means time (spatial) derivative. By use of these derivatives of θ_0 and ϕ_0 and keeping up to the second order of u and v, we obtain

$$L^1_\theta-\alpha L^2_\theta=-2R^1_\theta-2\kappa R^2_\theta+2dR^3_\theta,\tag{A2}$$

$$L^1_\varphi-\alpha L^2_\varphi=-2R^1_\varphi-2\kappa R^2_\varphi+2dR^3_\varphi,\tag{A3}$$

where

$$L^1_r=\lambda\frac{q_t}{\Delta}u\sin\theta_0+(\Gamma q_t-\phi_t)v\sin\theta_0-(uu_t+vv_t),\tag{A4}$$

$$\begin{aligned}L^1_\theta=&-\lambda\frac{q_t}{\Delta}\sin\theta_0+u_t+(\Gamma q_t-\phi_t)v\cos\theta_0\\&+\lambda\frac{q_t}{\Delta}\left[\frac{1}{2}\left(u^2+v^2\right)\right]\sin\theta_0,\end{aligned}\tag{A5}$$

$$\begin{aligned}L^1_\varphi=&-(\Gamma q_t-\phi_t)\sin\theta_0-(\Gamma q_t-\phi_t)u\cos\theta_0+v_t\\&+(\Gamma q_t-\phi_t)\left[\frac{1}{2}\left(u^2+v^2\right)\right]\sin\theta_0,\end{aligned}\tag{A6}$$

$$\begin{aligned}L^2_r=&-(\Gamma q_t-\phi_t)u\sin\theta_0+\lambda\frac{q_t}{\Delta}v\sin\theta_0\\&-(\Gamma q_t-\phi_t)\left(u^2+v^2\right)\cos\theta_0+uv_t-u_tv,\end{aligned}\tag{A7}$$

$$\begin{aligned}L^2_\theta=&(\Gamma q_t-\phi_t)\sin\theta_0+(\Gamma q_t-\phi_t)u\cos\theta_0-v_t\\&-(\Gamma q_t-\phi_t)u^2\sin\theta_0+\lambda\frac{q_t}{\Delta}uv\sin\theta_0,\end{aligned}\tag{A8}$$

$$\begin{aligned}L^2_\varphi=&-\lambda\frac{q_t}{\Delta}\sin\theta_0+u_t+(\Gamma q_t-\phi_t)v\cos\theta_0\\&+\lambda\frac{q_t}{\Delta}v^2\sin\theta_0-(\Gamma q_t-\phi_t)uv\sin\theta_0,\end{aligned}\tag{A9}$$

$$\begin{aligned}R^1_r=&\lambda\frac{2\Gamma}{\Delta}u\sin\theta_0\cos\theta_0-\left(\frac{1}{\Delta^2}-\Gamma^2\right)v\sin\theta_0\cos\theta_0\\&-\lambda\frac{2\Gamma}{\Delta}u^2\sin^2\theta_0+\left(\frac{1}{\Delta^2}-\Gamma^2\right)uv\sin^2\theta_0\\&+2\Gamma(uu_z+vv_z)\cos\theta_0+uv_{zz}-u_{zz}v,\end{aligned}\tag{A10}$$

$$\begin{aligned}R^1_\theta=&-\lambda\frac{2\Gamma}{\Delta}\sin\theta_0\cos\theta_0+\lambda\frac{2\Gamma}{\Delta}u\sin^2\theta_0-\frac{1}{\Delta^2}v\sin^2\theta_0\\&+\Gamma^2v\cos^2\theta_0-2\Gamma u_z\cos\theta_0-v_{zz}\\&+\lambda\frac{2\Gamma}{\Delta}\left(u^2+v^2\right)\sin\theta_0\cos\theta_0\\&-\left(\frac{1}{\Delta^2}+\Gamma^2\right)uv\sin\theta_0\cos\theta_0\\&+2\Gamma uu_z\sin\theta_0-2\frac{\lambda}{\Delta}u_zv\sin\theta_0,\end{aligned}\tag{A11}$$

$$\begin{aligned}R^1_\varphi=&\left(\frac{1}{\Delta^2}-\Gamma^2\right)\sin\theta_0\cos\theta_0-\Gamma^2u\cos2\theta_0+u_{zz}-2\Gamma v_z\cos\theta_0\\&-\left(\frac{1}{\Delta^2}-\Gamma^2\right)v^2\sin\theta_0\cos\theta_0+2\Gamma^2u^2\sin\theta_0\cos\theta_0\\&-2\frac{\lambda}{\Delta}vv_z\sin\theta_0+2\Gamma uv_z\sin\theta_0,\end{aligned}\tag{A12}$$

$$R^2_r=v\sin\theta_0\cos\theta_0-uv\sin^2\theta_0,\tag{A13}$$

$$R^2_\theta=v\cos^2\theta_0-uv\sin\theta_0\cos\theta_0,\tag{A14}$$

$$\begin{aligned}R^2_\varphi=&-\sin\theta_0\cos\theta_0-u\cos2\theta_0\\&+\left(2u^2+v^2\right)\sin\theta_0\cos\theta_0,\end{aligned}\tag{A15}$$

$$\begin{aligned}R^3_r=&\frac{\lambda}{\Delta}u\sin\theta_0\cos\theta_0+\Gamma v\sin\theta_0\cos\theta_0-\frac{\lambda}{\Delta}u^2\sin^2\theta_0\\&-\Gamma uv\sin^2\theta_0+(uu_z+vv_z)\cos\theta_0,\end{aligned}\tag{A16}$$

$$\begin{aligned}R^3_\theta=&-\frac{\lambda}{\Delta}\sin\theta_0\cos\theta_0+\frac{\lambda}{\Delta}u\sin^2\theta_0-u_z\cos\theta_0\\&+\Gamma v\cos^2\theta_0+\frac{\lambda}{\Delta}\left(u^2+v^2\right)\sin\theta_0\cos\theta_0\end{aligned}$$

$$-\Gamma uv\sin\theta_0\cos\theta_0+uu_z\sin\theta_0, \tag{A17}$$

$$R_\varphi^3=-\Gamma\sin\theta_0\cos\theta_0-\Gamma u\cos 2\theta_0-v_z\cos\theta_0 +\Gamma\left(2u^2+v^2\right)\sin\theta_0\cos\theta_0+uv_z\sin\theta_0. \tag{A18}$$

Based on the spin wave solutions of static domain wall (see Eqs. (11) and (12)), the spin waves around the dynamic DW should be expressed as $u=u(z-q(t),t)$ and $v=v(z-q(t),t)$. Hence, the derivatives with respective to time are $u_t=\frac{\partial u}{\partial t}-\frac{\partial u}{\partial z}q_t$ and $v_t=\frac{\partial v}{\partial t}-\frac{\partial v}{\partial z}q_t$. Substituting the expressions of u_t and v_t into the above equations, using the spin wave equations (9) and (10), and integrating over z, Eqs. (A2) and (A3) reduce to

$$\begin{aligned}&-\left[\int_{-\infty}^{\infty}\sin^2\theta_0\frac{\mathrm{d}z}{\Delta}+\lambda\Delta\int_{-\infty}^{\infty}(u_z+\alpha v_z)\sin\theta_0\frac{\mathrm{d}z}{\Delta}-1/2\int_{-\infty}^{\infty}\left(u^2+v^2\right)\sin^2\theta_0\frac{\mathrm{d}z}{\Delta}+\alpha\int_{-\infty}^{\infty}uv\sin^2\theta_0\frac{\mathrm{d}z}{\Delta}\right]\lambda q_t/\Delta\\&-\left[\alpha\int_{-\infty}^{\infty}\sin^2\theta_0\frac{\mathrm{d}z}{\Delta}+\int_{-\infty}^{\infty}(\alpha u-v)\sin\theta_0\cos\theta_0\frac{\mathrm{d}z}{\Delta}-\alpha\int_{-\infty}^{\infty}u^2\sin^2\theta_0\frac{\mathrm{d}z}{\Delta}\right](\Gamma q_t-\phi_t)\\&=4/\Delta^2\int_{-\infty}^{\infty}uv\sin^2\theta_0\cos\theta_0\frac{\mathrm{d}z}{\Delta}+4\lambda/\Delta\int_{-\infty}^{\infty}u_zv\sin^2\theta_0\frac{\mathrm{d}z}{\Delta},\end{aligned} \tag{A19}$$

$$\begin{aligned}&\left[\alpha\int_{-\infty}^{\infty}\sin^2\theta_0\frac{\mathrm{d}z}{\Delta}+\lambda\Delta\int_{-\infty}^{\infty}(\alpha u_z-v_z)\sin\theta_0\frac{\mathrm{d}z}{\Delta}-\alpha\int_{-\infty}^{\infty}v^2\sin^2\theta_0\frac{\mathrm{d}z}{\Delta}\right]\lambda q_t/\Delta\\&-\left[\int_{-\infty}^{\infty}\sin^2\theta_0\frac{\mathrm{d}z}{\Delta}+\int_{-\infty}^{\infty}(u+\alpha v)\sin\theta_0\cos\theta_0\frac{\mathrm{d}z}{\Delta}-1/2\int_{-\infty}^{\infty}\left(u^2+v^2\right)\sin^2\theta_0\frac{\mathrm{d}z}{\Delta}-\alpha\int_{-\infty}^{\infty}uv\sin^2\theta_0\frac{\mathrm{d}z}{\Delta}\right](\Gamma q_t-\phi_t)\\&=-4/\Delta^2\int_{-\infty}^{\infty}u^2\sin^2\theta_0\cos\theta_0\frac{\mathrm{d}z}{\Delta}+4\lambda/\Delta\int_{-\infty}^{\infty}v_zv\sin^2\theta_0\frac{\mathrm{d}z}{\Delta}.\end{aligned} \tag{A20}$$

Substituting the expressions of θ_0 and ϕ_0 into Eqs. (A19) and (A20), and after a tedious calculation of the integrals by Mathematica, the final q–ϕ equation (22) is obtained. Below Eq. (22), the integrals in the parameters a_{11}, a_{12}, a_{21}, a_{22}, b_1, and b_2 are listed as follows:

$$I_1=\pi\frac{\cos\left(\frac{\pi\Delta}{2\Lambda}\right)\cosh\left(\frac{\pi\Delta k}{2}\right)\left[\Delta k\sin(t\omega)-\left(\frac{\Delta}{\Lambda}+1\right)\cos(t\omega)\right]+\sin\left(\frac{\pi\Delta}{2\Lambda}\right)\sinh\left(\frac{\pi\Delta k}{2}\right)\left[\Delta k\cos(t\omega)+\left(\frac{\Delta}{\Lambda}+1\right)\sin(t\omega)\right]}{\cos\left(\frac{\pi\Delta}{\Lambda}\right)+\cosh(\pi\Delta k)}, \tag{A21}$$

$$I_2=\pi\frac{\sin\left(\frac{\pi\Delta}{2\Lambda}\right)\sinh\left(\frac{\pi\Delta k}{2}\right)\left[\Delta k\sin(t\omega)-\left(\frac{\Delta}{\Lambda}+1\right)\cos(t\omega)\right]-\cos\left(\frac{\pi\Delta}{2\Lambda}\right)\cosh\left(\frac{\pi\Delta k}{2}\right)\left[\Delta k\cos(t\omega)+\left(\frac{\Delta}{\Lambda}+1\right)\sin(t\omega)\right]}{\cos\left(\frac{\pi\Delta}{\Lambda}\right)+\cosh(\pi\Delta k)}, \tag{A22}$$

$$\begin{aligned}I_3=&\frac{2\pi}{3\left(\left(\frac{\Delta}{\Lambda}-1\right)^2+\Delta^2k^2\right)\left(\cos\left(\frac{2\pi\Delta}{\Lambda}\right)-\cosh(2\pi\Delta k)\right)}\\&\times\left\{\cos\left(\frac{\pi\Delta}{\Lambda}\right)\sinh(\pi\Delta k)\left[\Delta k\left(\frac{\Delta^2}{\Lambda^2}-\frac{2\Delta}{\Lambda}+\Delta^2k^2-1\right)\sin(2t\omega)-\frac{\Delta}{\Lambda}\left(\frac{\Delta^2}{\Lambda^2}+\Delta^2k^2+2\Delta k^2\Lambda-1\right)\cos(2t\omega)\right]\right.\\&\left.+\sin\left(\frac{\pi\Delta}{\Lambda}\right)\cosh(\pi\Delta k)\left[\Delta k\left(\frac{\Delta^2}{\Lambda^2}-\frac{2\Delta}{\Lambda}+\Delta^2k^2-1\right)\cos(2t\omega)+\frac{\Delta}{\Lambda}\left(\frac{\Delta^2}{\Lambda^2}+\Delta^2k^2+2\Delta k^2\Lambda-1\right)\sin(2t\omega)\right]\right\},\end{aligned} \tag{A23}$$

$$I_4=\frac{\pi}{3}\frac{\Delta}{\Lambda}\frac{1-\frac{\Delta^2}{\Lambda^2}+3\Delta^2k^2}{\left(1-\frac{\Delta}{\Lambda}\right)^2+\Delta^2k^2}\csc\left(\frac{\pi\Delta}{\Lambda}\right), \tag{A24}$$

$$\begin{aligned}I_5=&\frac{\pi}{3}\frac{\Delta}{\Lambda}\frac{1-\frac{\Delta^2}{\Lambda^2}+3\Delta^2k^2}{\left(1-\frac{\Delta}{\Lambda}\right)^2+\Delta^2k^2}\csc\left(\frac{\pi\Delta}{\Lambda}\right)-\frac{2\pi}{3\left[\left(\frac{\Delta}{\Lambda}-1\right)^2+\Delta^2k^2\right]\left[\cos\left(\frac{2\pi\Delta}{\Lambda}\right)-\cosh(2\pi\Delta k)\right]}\\&\times\left\{\sin\left(\frac{\pi\Delta}{\Lambda}\right)\cosh(\pi\Delta k)\left[\Delta k\left(\frac{\Delta^2}{\Lambda^2}-\frac{2\Delta}{\Lambda}+\Delta^2k^2-1\right)\sin(2t\omega)-\frac{\Delta}{\Lambda}\left(\frac{\Delta^2}{\Lambda^2}+\Delta^2k^2+2\Delta k^2\Lambda-1\right)\cos(2t\omega)\right]\right.\\&\left.-\cos\left(\frac{\pi\Delta}{\Lambda}\right)\sinh(\pi\Delta k)\left[\Delta k\left(\frac{\Delta^2}{\Lambda^2}-\frac{2\Delta}{\Lambda}+\Delta^2k^2-1\right)\cos(2t\omega)+\frac{\Delta}{\Lambda}\left(\frac{\Delta^2}{\Lambda^2}+\Delta^2k^2+2\Delta k^2\Lambda-1\right)\sin(2t\omega)\right]\right\},\end{aligned} \tag{A25}$$

$$\begin{aligned}I_6=&\frac{\pi}{3}\frac{\Delta}{\Lambda}\frac{1-\frac{\Delta^2}{\Lambda^2}+3\Delta^2k^2}{\left(1-\frac{\Delta}{\Lambda}\right)^2+\Delta^2k^2}\csc\left(\frac{\pi\Delta}{\Lambda}\right)+\frac{2\pi}{3\left[\left(\frac{\Delta}{\Lambda}-1\right)^2+\Delta^2k^2\right]\left[\cos\left(\frac{2\pi\Delta}{\Lambda}\right)-\cosh(2\pi\Delta k)\right]}\\&\times\left\{\sin\left(\frac{\pi\Delta}{\Lambda}\right)\cosh(\pi\Delta k)\left[\Delta k\left(\frac{\Delta^2}{\Lambda^2}-\frac{2\Delta}{\Lambda}+\Delta^2k^2-1\right)\sin(2t\omega)-\frac{\Delta}{\Lambda}\left(\frac{\Delta^2}{\Lambda^2}+\Delta^2k^2+2\Delta k^2\Lambda-1\right)\cos(2t\omega)\right]\right.\\&\left.-\cos\left(\frac{\pi\Delta}{\Lambda}\right)\sinh(\pi\Delta k)\left[\Delta k\left(\frac{\Delta^2}{\Lambda^2}-\frac{2\Delta}{\Lambda}+\Delta^2k^2-1\right)\cos(2t\omega)+\frac{\Delta}{\Lambda}\left(\frac{\Delta^2}{\Lambda^2}+\Delta^2k^2+2\Delta k^2\Lambda-1\right)\sin(2t\omega)\right]\right\},\end{aligned} \tag{A26}$$

$$I_7 = \pi\frac{\Delta}{\Lambda}\frac{1-\frac{\Delta^2}{\Lambda^2}+\Delta^2k^2}{\left(1-\frac{\Delta}{\Lambda}\right)^2+\Delta^2k^2}\Delta k\csc\left(\frac{\pi\Delta}{\Lambda}\right), \tag{A27}$$

$$I_8 = \pi\frac{\Delta^2}{\Lambda^2}\frac{\Delta^2k^2}{\left(1-\frac{\Delta}{\Lambda}\right)^2+\Delta^2k^2}\csc\left(\frac{\pi\Delta}{\Lambda}\right). \tag{A28}$$

Appendix B: The dynamic equation of q up to ρ^4

From Eq. (22), we can derive the dynamic equation of q up to ρ^4,

$$q_t = k\frac{E_0+E_1\rho\,\mathrm{e}^{-(q-q_s)/\Lambda}+E_2\rho^2\,\mathrm{e}^{-2(q-q_s)/\Lambda}}{F_0+F_2\rho^2\,\mathrm{e}^{-2(q-q_s)/\Lambda}+F_3\rho^3\,\mathrm{e}^{-3(q-q_s)/\Lambda}+F_4\rho^4\,\mathrm{e}^{-4(q-q_s)/\Lambda}}\rho^2\,\mathrm{e}^{-2(q-q_s)/\Lambda}, \tag{B1}$$

where

$$E_0 = 8\frac{1-\frac{\Delta^2}{\Lambda^2}+2\alpha\frac{\Delta}{\Lambda}\Delta k+\Delta^2k^2}{\left(1-\frac{\Delta}{\Lambda}\right)^2+\Delta^2k^2}\frac{\pi\Delta}{\Lambda}\csc\left(\frac{\pi\Delta}{\Lambda}\right), \tag{B2}$$

$$\begin{aligned}E_1 = {}& 4\lambda\pi\frac{\left(\frac{\Delta}{\Lambda}+1\right)^2+\Delta^2k^2}{\left(\frac{\Delta}{\Lambda}-1\right)^2+\Delta^2k^2}\frac{\frac{\pi\Delta}{\Lambda}\csc\left(\frac{\pi\Delta}{\Lambda}\right)}{\cos\left(\frac{\pi\Delta}{\Lambda}\right)+\cosh(\pi\Delta k)}\\ &\times\left\{\cos\left(\frac{\pi\Delta}{2\Lambda}\right)\cosh\left(\frac{\pi\Delta k}{2}\right)\left[\left(1-\frac{\Delta}{\Lambda}+\alpha\Delta k\right)\cos(t\omega)\right.\right.\\ &\left.-\left(\alpha\left(\frac{\Delta}{\Lambda}-1\right)+\Delta k\right)\sin(t\omega)\right]\\ &-\sin\left(\frac{\pi\Delta}{2\Lambda}\right)\sinh\left(\frac{\pi\Delta k}{2}\right)\left[\left(1-\frac{\Delta}{\Lambda}+\alpha\Delta k\right)\sin(t\omega)\right.\\ &\left.\left.+\left(\alpha\left(\frac{\Delta}{\Lambda}-1\right)+\Delta k\right)\cos(t\omega)\right]\right\},\end{aligned} \tag{B3}$$

$$\begin{aligned}E_2 = {}& \frac{4}{3}\frac{\left(\frac{\Delta^2}{\Lambda^2}-1-3\Delta^2k^2\right)\left(1-\frac{\Delta^2}{\Lambda^2}+\Delta^2k^2+2\alpha\frac{\Delta}{\Lambda}\Delta k\right)}{\left(\left(\frac{\Delta}{\Lambda}-1\right)^2+\Delta^2k^2\right)^2}\\ &\left[\frac{\pi\Delta}{\Lambda}\right]^2\csc^2\left(\frac{\pi\Delta}{\Lambda}\right)\\ &-\frac{8}{3}\pi\alpha\frac{\left(\frac{\Delta}{\Lambda}+1\right)^2+\Delta^2k^2}{\left[\left(\frac{\Delta}{\Lambda}-1\right)^2+\Delta^2k^2\right]^2}\frac{\frac{\pi\Delta}{\Lambda}\csc\left(\frac{\pi\Delta}{\Lambda}\right)}{\cos\left(\frac{2\pi\Delta}{\Lambda}\right)-\cosh(2\pi\Delta k)}\\ &\times\left\{\cos\left(\frac{\pi\Delta}{\Lambda}\right)\sinh(\pi\Delta k)\left[k\Delta\left(\frac{\Delta^2}{\Lambda^2}-1+\Delta^2k^2\right)\sin(2t\omega)\right.\right.\\ &\left.+\frac{\Delta}{\Lambda}\left(\left(\frac{\Delta}{\Lambda}-1\right)^2+\Delta^2k^2-2\Delta k\Lambda k\right)\cos(2t\omega)\right]\\ &+\sin\left(\frac{\pi\Delta}{\Lambda}\right)\cosh(\pi\Delta k)\left[k\Delta\left(\frac{\Delta^2}{\Lambda^2}-1+\Delta^2k^2\right)\cos(2t\omega)\right.\\ &\left.\left.-\frac{\Delta}{\Lambda}\left(\left(\frac{\Delta}{\Lambda}-1\right)^2+\Delta^2k^2-2\Delta k\Lambda k\right)\sin(2t\omega)\right]\right\},\end{aligned} \tag{B4}$$

with

$$F_0 = -4\left(\alpha^2+1\right), \tag{B5}$$

$$\begin{aligned}F_2 = {}& \frac{4}{3}\left(\alpha^2+1\right)\frac{1-\frac{\Delta^2}{\Lambda^2}+3\Delta^2k^2}{\left(\frac{\Delta}{\Lambda}-1\right)^2+\Delta^2k^2}\frac{\pi\Delta}{\Lambda}\csc\left(\frac{\pi\Delta}{\Lambda}\right)\\ &+2\pi^2\left(\alpha^2+1\right)\frac{\left(\frac{\Delta^2}{\Lambda^2}-1\right)^2+\Delta^2k^2\left[2\left(1+\frac{\Delta^2}{\Lambda^2}\right)+\Delta^2k^2\right]}{\left(\frac{\Delta}{\Lambda}-1\right)^2+\Delta^2k^2}\\ &\times\frac{1}{\cos\left(\frac{\pi\Delta}{\Lambda}\right)+\cosh(\pi\Delta k)},\end{aligned} \tag{B6}$$

$$\begin{aligned}F_3 = {}& -\frac{1}{3}\lambda\pi^2\alpha\frac{\left(\frac{\Delta}{\Lambda}+1\right)^2+\Delta^2k^2}{\left(\frac{\Delta}{\Lambda}-1\right)^2+\Delta^2k^2}\frac{1}{\cos\left(\frac{2\pi\Delta}{\Lambda}\right)-\cosh(2\pi\Delta k)}\\ &\times\left\{\sin\left(\frac{\pi\Delta}{2\Lambda}\right)\cosh\left(\frac{\pi\Delta k}{2}\right)\right.\\ &\times\left[\left(\frac{\Delta^2}{\Lambda^2}-\frac{\Delta}{\Lambda}+\Delta^2k^2+\alpha k\Delta\right)\sin(t\omega)\right.\\ &\left.+\left(\alpha\left(\frac{\Delta^2}{\Lambda^2}-\frac{\Delta}{\Lambda}+\Delta^2k^2\right)-k\Delta\right)\cos(t\omega)\right]\\ &-\cos\left(\frac{\pi\Delta}{2\Lambda}\right)\sinh\left(\frac{\pi\Delta k}{2}\right)\\ &\times\left[\left(\frac{\Delta^2}{\Lambda^2}-\frac{\Delta}{\Lambda}+\Delta^2k^2+\alpha k\Delta\right)\cos(t\omega)\right.\\ &\left.\left.-\left(\alpha\left(\frac{\Delta^2}{\Lambda^2}-\frac{\Delta}{\Lambda}+\Delta^2k^2\right)-k\Delta\right)\sin(t\omega)\right]\right\},\end{aligned} \tag{B7}$$

$$\begin{aligned}F_4 = {}& \frac{1}{9}\frac{1}{\left(\left(\frac{\Delta}{\Lambda}-1\right)^2+\Delta^2k^2\right)^2}\left\{-\alpha^2\left(k^2\Lambda^2+1\right)\right.\\ &\times\left[\left(\frac{\Delta^2}{\Lambda^2}-1\right)^2+\Delta^2k^2\left(2\left(1+\frac{\Delta^2}{\Lambda^2}\right)+\Delta^2k^2\right)\right]\\ &+\left[\alpha^2k^2\Lambda^2\left(1-3\frac{\Delta^2}{\Lambda^2}+\Delta^2k^2\right)^2\right.\\ &-3\Delta^2k^2\left(2\left(1-\frac{\Delta^2}{\Lambda^2}\right)+3\Delta^2k^2\right)\\ &\left.-\left(\frac{\Delta^2}{\Lambda^2}-1\right)^2\right]\cos\left(\frac{2\pi\Delta}{\Lambda}\right)\\ &\left.+\left(\alpha^2+1\right)\left(1-\frac{\Delta^2}{\Lambda^2}+3\Delta^2k^2\right)^2\cosh(2\pi\Delta k)\right\}\\ &\times\frac{\left[\frac{\pi\Delta}{\Lambda}\csc\left(\frac{\pi\Delta}{\Lambda}\right)\right]^2}{\cos\left(\frac{2\pi\Delta}{\Lambda}\right)-\cosh(2\pi\Delta k)}.\end{aligned} \tag{B8}$$

By solving Eq. (B1) numerically, we plot the dependence of velocity of domain wall on its distance from the source of spin

wave in Fig. B1.

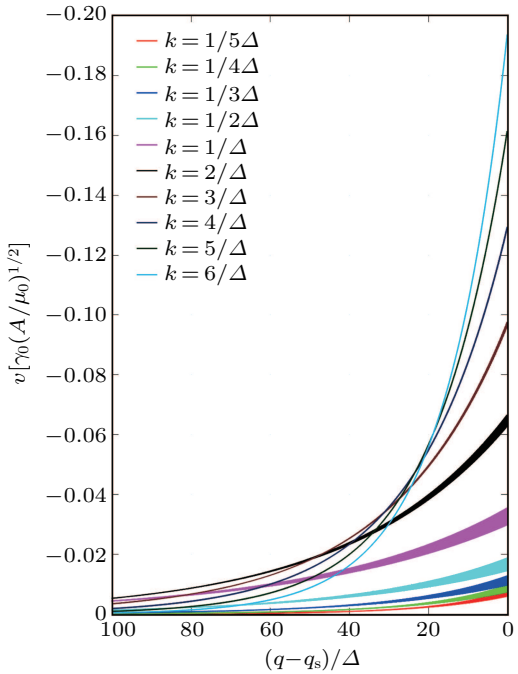


Fig. B1. Dependence of velocity of domain wall on its distance from the source of spin wave. The parameters are the same as those in Fig. 5 of the main text.

References

[1] Winter J M 1961 *Phys. Rev.* **124** 452
[2] Janak J F 1964 *Phys. Rev.* **134** A411
[3] Thiele A A 1973 *Phys. Rev. B* **7** 391
[4] Kishine J and Ovchinnikov A S 2011 *Phys. Lett. A* **375** 1824
[5] Borys P, Garcia-Sanchez F, Kim J V and Stamps R L 2016 *Adv. Electron. Mater.* **2** 1500202
[6] Bouzidi D and Suhl H 1990 *Phys. Rev. Lett.* **65** 2587
[7] Wieser R, Vedmedenko E Y and Wiesendanger R 2010 *Phys. Rev. B* **81** 024405
[8] Wang X S, Yan P, Shen Y H, Bauer G E W and Wang X R 2012 *Phys. Rev. Lett.* **109** 167209
[9] Woo S, Delaney T and Beach G S D 2017 *Nat. Phys.* **13** 448
[10] Whitehead N J, Horsley S A R, Philbin T G, Kuchko A N and Kruglyak V V 2017 *Phys. Rev. B* **96** 064415
[11] Macke S and Goll D 2010 *J. Phys.: Conf. Ser.* **200** 042015
[12] Yu W, Lan J, Wu R and Xiao J 2016 *Phys. Rev. B* **94** 140410
[13] Hämäläinen S J, Madami M, Qin H J, Gubbiotti G and van Dijken S 2018 *Nat. Commun.* **9** 4853
[14] Chang L J, Liu Y F, Kao M Y, Tsai L Z, Liang J Z and Lee S F 2018 *Sci. Rep.* **8** 3910
[15] Yanes R, Ontoso N, Torres L and Lopez-Diaz L 2019 *J. Phys. D: Appl. Phys.* **52** 175002
[16] Hertel R, Wulfhekel W and Kirschner J 2004 *Phys. Rev. Lett.* **93** 257202
[17] Bayer C, Schultheiss H, Hillebrands B and Stamps R L 2005 *IEEE Trans. Magn.* **41** 3094
[18] Buijnsters F J, Ferreiros Y, Fasolino A and Katsnelson M I 2016 *Phys. Rev. Lett.* **116** 147204
[19] Garcia-Sanchez F, Borys P, Soucaille R, Adam J P, Stamps R L and Kim J V 2015 *Phys. Rev. Lett.* **114** 247206
[20] Wagner K, Kákay A, Schultheiss K, Henschke A, Sebastian T and Schultheiss H 2016 *Nat. Nanotech.* **11** 432
[21] Yan P, Wang X S and Wang X R 2011 *Phys. Rev. Lett.* **107** 177207
[22] Kim J S, Stärk M, Kläui M, Yoon J, You C Y, Lopez-Diaz L and Martinez E 2012 *Phys. Rev. B* **85** 174428
[23] Wang X G, Guo G H, Nie Y Z, Zhang G F and Li Z X 2012 *Phys. Rev. B* **86** 054445
[24] Zhang S F, Mu C P, Zhu Q Y, Zheng Q, Liu X Y, Wang J B and Liu Q F 2014 *J. Appl. Phys.* **115** 013908
[25] Wang W W, Albert M, Beg M, Bisotti M A, Chernyshenko D, Cortés-Ortuno D, Hawke I and Fangohr H 2015 *Phys. Rev. Lett.* **114** 087203
[26] Li Z D, Li Q Y, Li L and Liu W M 2007 *Phys. Rev. E* **76** 026605
[27] Li Z D, Li Q Y, Xu T F and He P B 2016 *Phys. Rev. E* **94** 042220
[28] Zheng Z X, Li Q Y, Li Z D, Wang S X, Xu L P and Wen T D 2009 *Ann. Phys.* **324** 1612
[29] Han D S, Kim S K, Lee J Y, Hermsdoerfer S J, Schultheiss H, Leven B and Hillebrands B 2009 *Appl. Phys. Lett.* **94** 112502
[30] Wang X G, Guo G H, Zhang G F, Nie Y Z and Xia Q L 2013 *J. Appl. Phys.* **113** 213904
[31] Janutka A 2013 *IEEE Magn. Lett.* **4** 4000104
[32] H Hata H, Taniguchi T, Lee H W, Moriyama T and Ono T 2014 *Appl. Phys. Expr.* **7** 033001
[33] Moon K W, Chun B S, Kim W and Hwang C 2013 *J. Appl. Phys.* **114** 123908
[34] Wang X G, Guo G H, Zhang G F, Nie Y Z and Xia Q L 2013 *Appl. Phys. Lett.* **102** 132401
[35] Risinggård V, Tveten E G, Brataas A and Linder J 2017 *Phys. Rev. B* **96** 174441
[36] Tretiakov O A and Abanov Ar 2010 *Phys. Rev. Lett.* **105** 157201
[37] Zhuo F J and Sun Z Z 2016 *Sci. Rep.* **6** 25122
[38] Blundell S 2001 *Magnetism in Condensed Matter* (London: Oxford Press) p. 86
[39] Aharoni A 1998 *J. Appl. Phys.* **83** 3432
[40] Zakeri Kh, Zhang Y, Prokop J, Chuang T H, Sakr N, Tang W X and Kirschner J 2010 *Phys. Rev. Lett.* **104** 137203
[41] Moon J H, Seo S M, Lee K J, Kim K W, Ryu J, Lee H W, McMichael R D and Stiles M D 2013 *Phys. Rev. B* **88** 184404
[42] Cortés-Ortuño D and Landeros P 2013 *J. Phys.: Condens. Matter* **25** 156001
[43] Garcia-Sanchez F, Borys P, Vansteenkiste A, Kim J V and Stamps R L 2014 *Phys. Rev. B* **89** 224408
[44] Lekner J 2007 *Am. J. Phys.* **75** 1151
[45] Malozemoff A P and Slonczewski J C 1979 *Magnetic Domain Walls in Bubble Materials* (New York: Academic Press) pp. 79–80